Utilizing optical spectroscopy and 2′,7′-difluorofluorescein to characterize the early stages of cement hydration

To cite this article: J Pauli *et al* 2022 *Methods Appl. Fluoresc.* **10** 015001

Methods and Applications in Fluorescence

OPEN ACCESS

RECEIVED
19 April 2021

REVISED
2 August 2021

ACCEPTED FOR PUBLICATION
7 October 2021

PUBLISHED
28 October 2021

PAPER

Utilizing optical spectroscopy and 2′,7′-difluorofluorescein to characterize the early stages of cement hydration

J Pauli[1], **A Ramírez**[1,2], **C Crasselt**[2], **W Schmidt**[2] **and U Resch-Genger**[1,*]

[1] Division Biophotonics, Bundesanstalt für Materialforschung und -prüfung (BAM), Richard-Willstaetter Str. 11, D-12489 Berlin, Germany

[2] Division Technology of Construction Materials, Bundesanstalt für Materialforschung und -prüfung (BAM), Unter den Eichen 87, D-12205 Berlin, Germany

[*] Author to whom any correspondence should be addressed.

E-mail: ute.resch@bam.de

Keywords: cement, optical spectroscopy, fluorescence, 2′, 7′-difluorofluorescein, cement hydration

Supplementary material for this article is available online

Abstract

The increasingly sophisticated nature of modern, more environmentally friendly cementitious binders requires a better understanding and control particularly of the complex, dynamic processes involved in the early phase of cement hydration. In-situ monitoring of properties of a constantly changing system over a defined period of time calls for simple, sensitive, fast, and preferably also non-invasive methods like optical spectroscopy. Here, we exploit the time-dependent changes in the absorbance and fluorescence features of the negatively charged optical probe 2′,7′-difluorofluorescein (DFFL) for the study of the hydration processes in pastes of white cement (WC), cubic tricalcium aluminate (C_3A), and tricalcium silicate (C_3S), the main phases of cement, and in pastes of quartz (Q) over 24 h after addition of the dye solution. For comparison, also conventional techniques like isothermal heat flow calorimetry were applied. Based upon the time-dependent changes in the spectroscopic properties of DFFL, that seem to originate mainly from dye aggregation and dye-surface interactions and considerably vary between the different pastes, molecular pictures of the hydration processes in the cement pastes are derived. Our results clearly demonstrate the potential of optical spectroscopy, i.e., diffuse reflectance, steady state and time-resolved fluorometry in conjunction with suitable optical reporters, to probe specific hydration processes and to contribute to a better understanding of the early hydration processes of cement at the molecular scale.

Introduction

The development of building materials with significantly lower CO_2-footprint is one of the main challenges of the 21st century as the construction business contributes to about 40% of the global anthropogenic carbon emissions [1]) to which cement industry contributes mostly with around 8% [2, 3]. The main component of cement is clinker, to which a defined amount of a calcium sulfate (gypsum $CaSO_4{}^*2H_2O$, hemihydrate $CaSO_4{}^*1/2H_2O$, anhydrite $CaSO_4$) is added as a setting regulator to avoid flash setting. Clinker consists of four main phases: tricalcium silicate ($C_3S = Ca_3SiO_5$ = Alite), which constitutes the largest part of clinker (45–80 wt.%), followed by dicalcium silicate ($C_2S = Ca_2SiO_4$ = Belite) (0–32 wt.%), tricalcium aluminate ($C_3A = Ca_3Al_2O_6$) (4–14 wt.%%), and tetracalcium alumino ferrite ($C_4AF = Ca_4Al_2Fe_2O_{10}$) (7–15 wt.%) [4]. C_3S and C_2S react with water to calcium silicate hydrate (C–S–H) and portlandite ($Ca(OH)_2$), which determines the stiffness and strength of concrete. The reaction of C_3A with water significantly contributes to the workability and the slump life of fresh concrete [5–8].

Established analytical methods to study the processes during cement hydration include isothermal heat flow calorimetry [9–11], *in situ* XRD [5, 12–14], solid-state NMR [15–18], NMR relaxometry [19, 20], ATR-FTIR spectroscopy [21] and Raman spectroscopy [22–24]. As indicated by calorimetry, the strongly exothermic hydration of cement [9, 25, 26] can be

separated in four main phases, namely (i) a short and strongly exothermic hydration process upon contact with water that is characterized by the dissolution of aluminum-rich clinker phases and slows down within a few minutes, (ii) an induction period, that lasts from a few minutes to typically a few hours, at the onset of which the hydration rate rapidly decreases, (iii) a third period of several hours, during which a scaffold of C–S–H–sheet structures form, portlandite and ettringite crystals grow, and the voids between cement particles start to fill, all leading to the setting of cement, and (iv) the continuous hydration, where the hydration process is assumed to be controlled by either slower diffusion or space filling [11]. During this fourth phase, that lasts for several hours depending on the cement composition, the water to cement ratio and the used admixtures, cement hardening increases and the pore diameter between the cement particles gradually decreases with time.

Although the structural changes in the first stage of cement hydration have been assessed with different analytical methods before, an in-depth understanding of the processes occurring during cement hydration at the molecular level requires analytical methods that enable to continuously study the hydration processes *in situ* in real time without the need to stop the hydration process. This calls for optical methods like reflectance and fluorescence spectroscopy. Optical methods, that often utilize reporters with specifically chosen absorption and/or emission properties for signal generation, have been successfully used for the analysis and *in situ* monitoring of the interactions between a broad variety of nanoscale and molecular systems, and chromophore-surface interactions [27–38]. Examples for the latter present textile dyeing and the production of colored ceramics [39, 40], the staining of tissue sections or selected cell organelles in forensics [41] as a prerequisite for the analysis with fluorescence microscopy [42–44], and the characterization of clay surfaces [29, 36, 45]. Encouraged by first studies on the early stages of the hydration of C3A pastes probed with a water soluble fluorescent cyanine dye and the good correlation between the changes in the optical properties of this reporter dye with the results of XRD measurements [27, 28], we expanded these investigation now to the distinction between different cement phases, here using less expensive and broadly used 2′,7′-difluorofluorescein (DFFL) [46–50]. This dye was chosen here as it is very water soluble, has a high molar absorption coefficient and a higher fluorescence quantum yield than our previously used cyanine dye S0586, thus enabling even more sensitive optical measurements. DFFL is stable at basic pH values above 12 and high ionic strength as characteristic for cement-water systems and has pH-responsive absorption and emission features. Moreover, this fluorophore is negatively charged while calcium aluminates (C_3A, C_4AF, and ettringite) [51–53], as well as calcium silicates (C_3S, C–S–H) present in the pore solutions [52, 54, 55] are characterized by positive zeta-potentials. As the calculation of the dye absorbance in the presence of gray colored conventional Portland cement with its gray color is challenging (the reflectance of such a gray paste is between 11 and 17 percent depending on the detection wavelength), for the optical studies, only pastes of white cement (WC), a Portland cement with a very low amount of Fe_2O_3, were used. In addition, also pastes of the pure main phases of WC, namely C_3S and cubic C_3A, were analyzed, as well as pastes of a relatively inert quartz filler (Q), that are subsequently referred to as WC-DFFL, C_3S-DFFL, C_3A-DFFL, and Q-DFFL pastes.

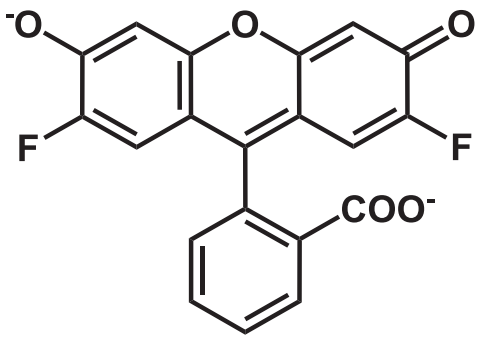

Figure 1. Chemical structure of deprotonated 2′,7′-difluorofluorescein (DFFL) as formed at pH > 6 [47] adapted with permission from A. Orte, L. Crovetto, E. M. Talavera, N. Boens and J. M. Alvarez-Pez, Journal of Physical Chemistry A, 2005, 109, 734–747 Copyright 2021 American Chemical Society.

Experimental

Materials

All materials were used as received. White cement was obtained from CEMEX Deutschland AG (CEM I 42,5 R (dw)), tricalcium aluminate ($3CaO.Al_2O_3$) and tricalcium silicate ($3CaO{\cdot}SiO_2$) from VUSTAH, Research Institute for Building Materials, Brno, quartz filler from Euroquarz, $Ca(OH)_2$ from CHEMSOLUTE, and KOH from PanReac AppliChem ITW Reagents, respectively. Microscopic slides and glass plates were purchased from Menzel Gläser, and UHU PLUS 2 k-epoxy glue (curation time = 5 min) from UHU GmbH & Co (Bolton Adhesive Group). The chemical structure of the dye 2′,7′-difluorofluorescein (DFFL; Oregon Green^{TM} 488) [46, 47, 49], purchased from Fisher Scientific GmbH, is shown in figure 1.

The composition of WC was determined on the basis of the X-ray Rietveld spectra and applying of the Match! Software with the PDF2-2003 database [56] and is summarized in table 1.

Table 1. Composition of the white cement used in this study.

Component	Weight percentage of the component in white cement/%
C_3S	57.3
C_2S	23.6
C_3A	8.1
C_4AF	0
$CaSO_4$ (Anhydrite)	10.1
$Ca(OH)_2$	0.9

Sample preparation for diffuse reflectance and fluorescence measurements

0.31 mg DFFL were dissolved in 2.66 ml $Ca(OH)_2$-solution ($c_{DFFL} = 3.2^{*}10^{-4}$ M) obtained by dissolving 2.7 mg $Ca(OH)_2$ in 50 ml milli-Q-water ($C_{ca(HO)2} = 0.73$ mM, pH = 11.3). DFFL is stable under these conditions for more than 24 h (see figure S1 (available online at stacks.iop.org/MAF/10/015001/mmedia) in the Supporting Information (SI)). At this pH, DFFL has a molar absorption coefficient of 36,000 $lmol^{-1}\,cm^{-1}$ at the excitation wavelength of 465 nm (92,000 $lmol^{-1}\,cm^{-1}$ at the absorption maximum at 490 nm) and a very high fluorescent quantum yield of 0.9 (see table S1 in the supporting information).

A water (w) to solid (s) mass ratio (w/s) of 0.5 was used for the WC-DFFL and C_3S-DFFL pastes. The w/s ratio was increased to 1 for the preparation of a homogeneous C_3A-DFFL paste, because C_3A immediately reacted with water and no homogenous paste could be prepared at a lower w/s ratio. The Q-DFFL pastes had to be prepared with a w/s ratio of 0.25 due to the consistence of the pastes as the samples had to be positioned vertically in the spectrometers and therefore should not be too liquid.

22 mg of the dry powder (WC, Q, C_3A, C_3S) were placed on a microscopic slide (26 × 76 mm, with indentation of 1.20–1.50 mm) and 11 μl of basic dye solution (for WC-DFFL, C_3S-DFFL), 22 μl (for C_3A-DFFL) or 5.5 μl (for Q-DFFL) was added. The pastes were manually mixed for 2 min, before the mixture was covered with a glass plate (20 mm × 20 mm), which was fixed with epoxy resin to prevent the evaporation of water or the carbonation of the pastes. Each paste was prepared at least four times, whereby two examples were used for fluorescence measurements and the other two for reflectance measurements, respectively.

Optical methods

UV–Vis diffuse reflectance spectra (UV-VisDR)

The absorption properties of optically not transparent cement pastes are only accessible by diffuse reflectance measurements and the subsequent calculation of these features using the Kubelka-Munk function (KM absorbance) [57–62]. UV-VisDR spectra were recorded with a Perkin-Elmer LAMBDA 900 spectrophotometer in the wavelength range of 300 nm to 2200 nm over a period of 24 h in intervals of 20 min The Perkin-Elmer LAMBDA 900 spectrophotometer is equipped with a tungsten lamp, a double monochromator, an integrating sphere with a diameter of 150 mm, and two detectors, i.e., a photomultiplier tube PMT R-955 and a PbS detector, located at the bottom of the integrating sphere. The integrating sphere was operated in a double beam mode. Short pass filters with cut-off wavelengths of 500 nm (SP500) and 525 nm (SP525) were used to suppress a contribution of dye fluorescence to the measured reflectance spectra (see SI, figure S4). The filter SP500 assures the complete suppression of fluorescence of the used dye and allows the determination of its maximum absorbance, but partly distorts the signal form of the calculated absorbance spectra (see SI, figure S5). Therefore, additional measurements with filter SP525 were done to enable the analysis of the shape of the absorbance signals. A calibrated Spectralon® reflectance standard SRS-60-010 from Labsphere was used as a standard for 60% reflectance. The slides containing the cement pastes were placed outside of the integrated sphere at a port with an angle of 8°. The diffuse reflectance data were converted to Kubelka-Munk function values (F(R∞)) according to the Kubelka–Munk equation (see (equation (1))) [57–59, 61]. In equation (1), F(R∞) equals the quotient of the absorption coefficient (k) and the scattering coefficient (s) at a selected wavelength.

$$F(R_\infty) = \frac{(1 - R_\infty)^2}{2 * R_\infty} = \frac{k}{s} \quad (1)$$

The absorption coefficient k is proportional to the concentration of the dye (see (equation (2)).

$$k \sim \varepsilon * c \quad (2)$$

The absorbance signal (KM) of the dye in the pastes was obtained from the difference of the absorbance spectra (KM) of the dye-containing pastes and the spectra of the respective pastes without dye.

Fluorescence emission spectra

Emission spectra were measured with a calibrated Edinburgh fluorometer (FSP920) in a front face geometry in a spectral window of 475 nm to 725 nm employing an excitation wavelength of 465 nm. These measurements were performed in intervals of 20 min over a period of 24 h whereby complete fluorescence spectra were measured. Subsequently, the fluorescence intensity at the emission maximum of each spectrum was plotted as a function of hydration time.

Time-resolved fluorescence measurements

The fluorescence decay curves of the pastes were measured with a calibrated Edinburgh fluorometer (FLS920) in a front face geometry employing an excitation wavelength of 465 nm of the SuperK Fianium-laser FIU-15 from NKT Photonics and a

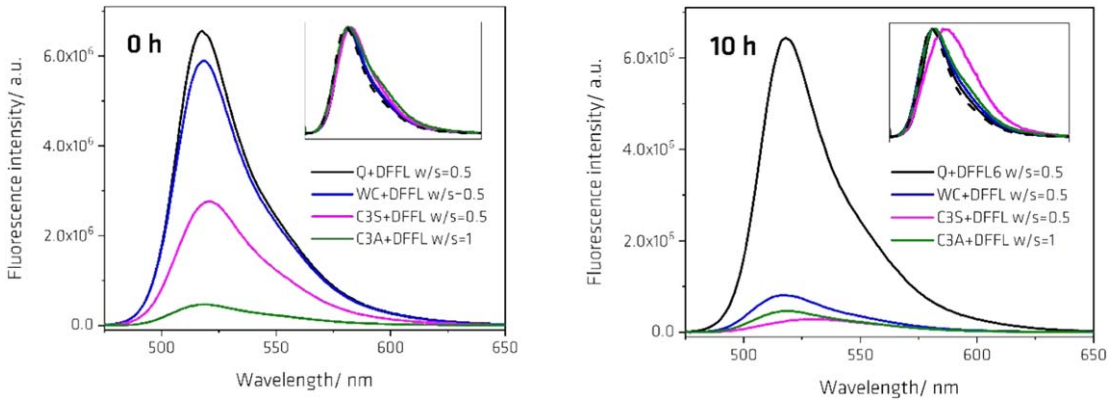

Figure 2. Fluorescence spectra of DFFL in the pastes of Q (w/s = 0.5), WC (w/s = 0.5), C_3S (w/s = 0.5) and C_3A (w/s = 1), measured 10 min (left) and 10 h (right) after paste preparation. Inset: Normalized emission spectra of the pastes and a DFFL solution (dashed line, pH = 12.6).

detection wavelength of 525 nm. The fluorescence lifetimes of the samples were obtained from the recorded decay curves after deconvolution of the instrument response function (IRF) utilizing the software package FAST (Fluorescence Analysis Software Technology) from Edinburgh Instruments. The IRF was measured with a diluted Ludox® HS-40 colloidal silica suspension in water (Aldrich Chemistry) excited at 465 nm. The concentration of the component c_1 with the lifetime τ_1 was calculated according to (equations (3) and (4)), whereby R(t) describes the exponential fit of a fluorescence decay curve with two exponential terms and the weighting factors B_1 and B_2, respectively.

$$c_{sh} = \frac{B_1}{B_1 + B_2} \tag{3}$$

$$R(t) = B_1 e^{-\frac{t}{\tau_1}} + B_2 e^{-\frac{t}{\tau_2}} \tag{4}$$

The concentration c_{sh} of the components with the two shortest lifetime s τ_1 and τ_2 was calculated according to (equations (3) and (4)), whereby R(t) describes the exponential fit of a fluorescence decay curve with three exponential terms and the weighting factors B_1, B_2 and B_3, respectively.

$$c_{sh} = \frac{(B_1 + B_2)}{B_1 + B_2 + B_3} \tag{5}$$

$$R(t) = B_1 e^{-\frac{t}{\tau_1}} + B_2 e^{-\frac{t}{\tau_2}} + B_3 e^{-\frac{t}{\tau_2}} \tag{6}$$

X-ray diffraction (XRD)

To characterize and quantify the mineral phases formed during cement hydration, XRD measurements were performed with a Bragg–Brentano geometry Rigaku Ultima IV diffractometer under the following conditions: CuKα radiation (λ = 1.541874 Å), 40 kV, 40 mA; sampling interval: 0.05° 2θ; scan rate: 3.3° 2θ min^{-1}; scanning range: 7°– 37° 2θ; divergence slit: in-plane 0.5°, axial 10 mm; strip detector D/teX Ultra with 5° Soller slits. The calibration of the diffractometer was done using a Si polycrystal. The qualitative phase identification was achieved with the Match! Software with the PDF2-2003 database [56].

Isothermal heat flow calorimetry

The isothermal heat release was determined with a TAM Air calorimeter from Thermometric AG, Sweden. Pastes were prepared using White cement and deionized water at a water to cement ratio of 0.5 and subsequent mixing for 2 min 15 g of this paste was employed for the calorimetric measurements at 20 °C.

Results and discussion

Analysis of pastes with fluorescence spectroscopy

In the freshly prepared pastes (t = 0 h), the fluorescence intensity of the dye DFFL decreased from the pastes of Q-DFFL (w/s = 0.5), over WC-DFFL (w/s = 0.5) and C_3S-DFFL (w/s = 0.5) to C_3A-DFFL (w/s = 1) reaching values of 77% in the WC-DFFL pastes, 46% in the C_3S-DFFL pastes, and 5% in the C_3A-DFFL pastes relative to the maximum fluorescence intensity of DFFL in the Q-DFFL pastes (see figure 2, left). Interesting is the low fluorescence intensity of DFFL in the C_3A-DFFL pastes considering the higher dye concentration used, exceeding that utilized for the other pastes by a factor of 2. 10 h after paste preparation (see figure 2, right), the fluorescence intensity of DFFL in Q-DFFL paste was still unaffected while for the WC-DFFL and C_3S-DFFL pastes, it considerably decreased during the first 10 h.

The time-dependent changes in the maximum fluorescence intensity of DFFL in the Q-DFFL, WC-DFFL, C_3S-DFFL, and C_3A-DFFL pastes are summarized in figure 3. The curves were normalized at the respective initial fluorescence intensities (t = 0 h), that differed (see figure 2) for a better visualization of the differences in the respective time-dependent changes.

The DFFL fluorescence in the WC-DFFL pastes decreased after 4.5 h and reached a constant value after

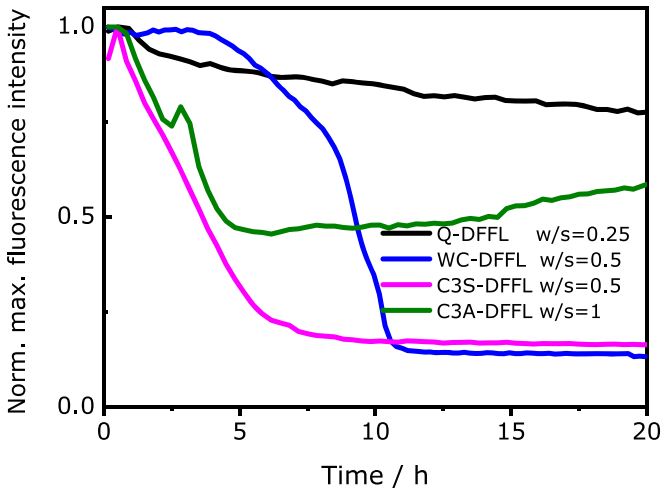

Figure 3. Time course of the maximum fluorescence intensities of DFFL in pastes of Q-DFFL (w/s = 0.25, black), WC-DFFL (w/s = 0.5, blue), C_3S-DFFL (w/s = 0.5, pink), and C_3A-DFFL (w/s = 1, green), normalized to 1.

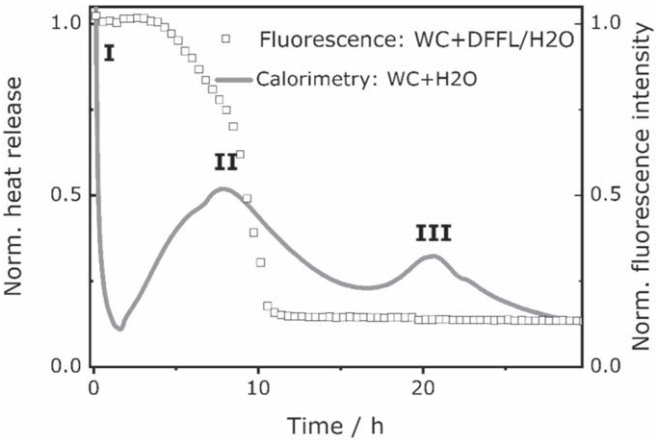

Figure 4. Time-dependent normalized heat release of a WC-paste with w/s=0.5 and the time-course of DFFL fluorescence intensity in WC-DFFL pastes.

Table 2. Spectral position of the emission maximum of DFFL in the pastes of Q-DFFL, WC-DFFL, C_3S-DFFL, and C_3A-DFFL at different reaction times. The emission maximum of DFFL in a saturated $Ca(OH)_2$ solution is located at 514 nm.

Sample/time	t = 0 h	t = 10 h	t = 20 h
Quartz	518 nm	518 nm	518 nm
White cement	519 nm	518 nm	518 nm
C_3S	523 nm	529 nm	529 nm
C_3A	518 nm	518 nm	518 nm

10.5 h, equaling approximately 15% of the initial fluorescence intensity. In contrast, the fluorescence intensity of DFFL in the C_3S-DFFL pastes decreased very rapidly after a short increase in the beginning of the hydration. After 6 h, the intensity was only 15% of the starting value. The maximum fluorescence intensity of DFFL in the Q pastes also decreased moderately with time. The spectral position of the emission maxima of DFFL in the Q-DFFL, WC-DFFL, C_3S-DFFL, and C_3A-DFFL pastes obtained at the beginning of the hydration process, after 10 h and 20 h are summarized in table 2. Apparently, only for the C_3S-DFFL paste, bathochromic spectral shifts occur.

Comparison of time-dependent fluorescence intensity changes with isothermal heat flow calorimetry results.

Figure 4 summarizes the time course of the fluorescence intensity of DFFL in the WC-DFFL pastes and the isothermal heat flow calorimetry results obtained with this WC paste without DFFL. The heat flow curve shows typical peaks and shoulders related to cement hydration as reported in the literature [9]. The second maximum is assigned to the point of deceleration of the fast growth of calcium silicate hydrates (C–S–H) [10, 20, 26]. Apparently, with the onset of formation of C–S–H, the maximum fluorescence intensity of DFFL starts to decrease. We attribute this drop in DFFL fluorescence to DFFL adsorption at or intercalation

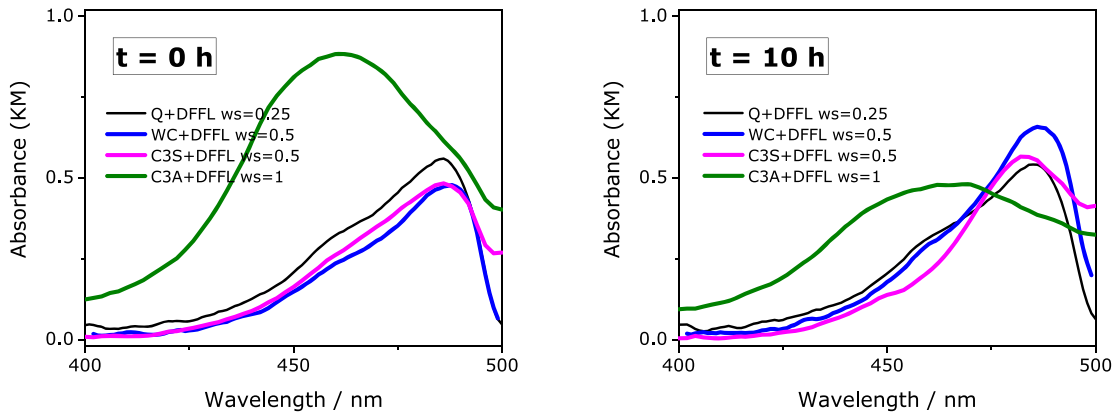

Figure 5. Absorbance spectra (KM) at t = 0 h (left) and t = 10 h (right) of the WC-DFFL and C_3S-DFFL pastes (w/s = 0.5), the C_3A-DFFL pastes (w/s = 1), and the Q-DFFL (w/s = 0.25) measured with a cut-off filter of 500 nm.

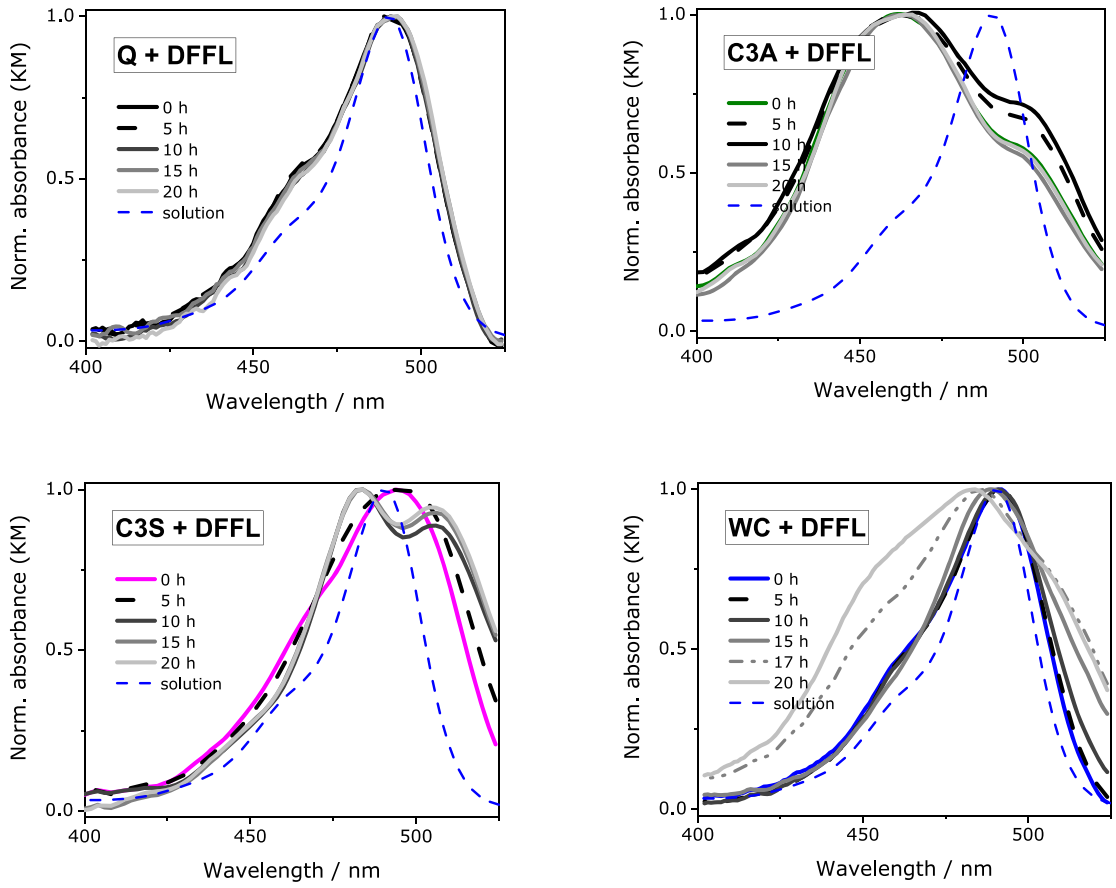

Figure 6. Normalized absorbance spectra (KM) of the pastes prepared from Q (first row, left), C_3A (first row, right), C_3S (second row, left), and WC (second row, right) at different times of hydration and the absorbance spectrum of DFFL in saturated $Ca(OH)_2$ solution (dashed line). The measurements were done with a cut-off filter of 525 nm.

[63] into calcium-silicate-hydrates, see also discussion in the following sections.

Diffuse reflectance spectroscopy

To discriminate between the different possible processes affecting DFFL fluorescence like the interaction with surfaces, i.e., of cement particles or hydrates, dye-dye interaction (dye aggregation) promoted by cations like Ca^{2+}, specific dye-metal ion interactions, and a decomposition of DFFL, we performed time-dependent diffuse reflectance measurements with the different pastes.

The absorbance spectra (KM) obtained from the diffuse reflectance spectra measured at the beginning of the paste hydration (t = 0 h) and after 10 h are shown in figure 5. The most intense signal results for DFFL in the C_3A-pastes at t = 0 h as to be expected from the higher amount of DFFL used. After 10 h of

Table 3. Maxima (max) and shoulders (sh) of the absorbance spectra (KM) of DFFL in pastes of Q, WC, C_3S and C_3A at different times.

Sample/time	t = 0 h	t = 10 h	t = 20 h
Quartz filler	491 nm	491 nm	491 nm
White cement	490 nm	490 nm	484 nm(max)/ 450 nm(sh)/510 nm(sh)
C_3S	494 nm	484 nm(max)/ 506 nm(max)	484 nm(max)/ 506 nm(max)
C_3A	462 nm(max)/ 500 nm(sh)	462 nm(max)/ 500 nm(sh)	462 nm(max)/ 500 nm(sh)

hydration, the DFFL absorbance (KM) in all four pastes is comparable.

The time courses of the normalized absorbance spectra (KM) of DFFL in the WC-DFFL, C_3S-DFFL, and C_3A-DFFL pastes as well as in the pastes of Q-DFFL in the first 24 h of hydration are summarized in figure 6, For comparison, also the absorbance spectrum of DFFL in a saturated $Ca(OH)_2$ solution ($3 * 10^{-4}$ M DFFL) is shown, revealing a broadening of the dye's absorbance band in all pastes. Interestingly, the DFFL absorbance bands in the different pastes differ in shape. Except for the C_3A-DFFL pastes, revealing an absorption maximum at 462 nm, the spectral position of the absorbance maxima (KM) of DFFL in the pastes is nearly the same as found in solution (490 nm). Furthermore, the absorbance spectrum of DFFL in the C_3A-DFFL pastes shows a shoulder at 500 nm. While the shape and spectral position of the absorbance spectrum (KM) of C_3A-DFFL and Q-DFFL did not change with time, the absorbance spectra (KM) of DFFL in the C_3S-DFFL and WC-DFFL pastes are time-dependent. After 10 h of hydration, the DFFL absorbance band in the C_3S-DFFL pastes splits into two bands with maxima at 484 nm and 506 nm. The absorbance band of DFFL in the WC-DFFL pastes starts to change 15 h after the beginning of hydration, the band maximum shifts to 484 nm and two shoulders appear, one at 450 nm and one at 510 nm, respectively. The spectral position of the absorbance spectra of DFFL in the different pastes at 0 and 20 h after the beginning of the hydration process are summarized in table 3.

Fluorescence lifetime measurements

After having determined the spectral position of the absorbance maxima of DFFL in the different pastes, we performed time-resolved fluorescence measurements with the dye in solution, in freshly prepared pastes, and in pastes after hydration times of 10 h and 24 h. These measurements provide the dye- and environment-specific parameters fluorescence lifetime (see table 4), which correlates with the fluorescence quantum yield, and the fluorescence decay kinetics. The latter can provide a hint on the microenvironment of DFFL and the interaction of the dye with its microenvironment. For example, in an aqueous environment, DFFL reveals mono-exponential decay kinetics that can become bi- or tri-exponential (see (equations (4) or (6))) in a more heterogeneous surrounding or by interaction with particle surfaces [64–66]. A shortening of the fluorescence lifetime can indicate dynamic fluorescence quenching and an increase in fluorescence lifetime, e.g. dye rigidization while static fluorescence quenching mainly affects only the resulting fluorescence intensity [67]. As summarized in table 4, DFFL reveals mono-exponential decay kinetics and a single fluorescence lifetime in basic solution, in all Q pastes studied, and in freshly prepared pastes of WC. Apparently, under these conditions, the DFFL molecules are located in an aqueous environment. The changes in the decay kinetics and fluorescence lifetimes observed for the other samples point to an increasingly heterogeneous dye microenvironment, suggesting dye-dye interactions and/or interactions of DFFL with surface of, e.g., cement particles.

Evaluating the observed time-dependent changes in the spectroscopic properties of DFFL

Possible explanations for the time-dependent changes in the spectral position, shape, and intensity of the fluorescence and absorbance spectra of DFFL, described in the previous sections, are summarized in table 5. Possible effects responsible for the observed spectroscopic changes include (a) interactions (i.e., adsorptive, electrostatic or hydrogen bonding interactions) of DFFL molecules with the surface of particles formed during the hydration process [29, 64–66, 68, 69], (b) dye dimerization and aggregation induced by local changes in dye concentration due to water consumption [70–77], (c) changes in the polarity and ionic strength of the dye microenvironment [49, 78–81], and (d) a decrease of the pH value [46–49]. In addition, DFFL can also decompose, resulting in a loss in fluorescence and absorbance.

For the interpretation of our previously described observations, additional experiments were done, specifically assessing the influence of dye concentration as well as pH and ionic strength (modelling, e.g., pore solutions) on the optical properties of DFFL. The resulting spectroscopic data are summarized in the SI (see chapter 2–3). These results reveal that the main spectroscopic changes occurring in the different pastes immediately after mixing with the dye solution (at times of 0 h) and after 24 h, which are summarized in

Table 4. Fluorescence decay kinetics and lifetimes of DFFL in solution and in different pastes at different hydration times as well as the parameter $\chi 2$ as a measure for fit quality and the relative concentration of the component with the shortest lifetime(s) c_{short}.

Paste/solution	w/s	Time/h	λ_{ex}/nm	Lifetime/ns	$\chi 2$	c_{short}
DFFL in $Ca(OH)_2/H_2O$		0	465	4.6	1.316	
Q-DFFL	0.5	0	465	4.9	1.268	
Q-DFFL	0.5	10	465	4.6	1.309	
Q-DFFL	0.5	24	465	4.6	1.317	
Q-DFFL	0.5	24	490	4.6	1.361	
Q-DFFL	0.5	24	510	4.6	1.316	
WC-DFFL	0.5	0	465	4.4	1.414	
WC-DFFL	0.5	10	465	1.3/4.2	1.316	9
WC-DFFL	0.5	24	465	1.0/3.6	1.409	21
WC-DFFL	0.5	24	450	0.8/3.5	1.528	21
WC-DFFL[a]	0.5	24	450	0.3/2.0/3.7	1.325	36[a]
WC-DFFL[a]	0.5	24	484	0.4/1.9/3.7	1.32	30[a]
WC-DFFL[a]	0.5	24	510	0.2/1.4/3.5	1.364	52[a]
C_3A-DFFL	1	0	465	0.8/3.6	1.307	7
C_3A-DFFL	1	10	465	0.8/3.6	1.45	24
C_3A-DFFL	1	24	465	0.7/3.6	1.55	34
C_3A-DFFL[a]	1	24	465	0.3/1.5/3.8	1.283	44
C_3A-DFFL	1	24	500	0.3/1.4/3.7[a]	1.271	54[a]
C_3S-DFFL	0.5	0	465	0.6/4.1	1.328	23
C_3S-DFFL	0.5	10	465	0.7/3.2	1.817	36
C_3S-DFFL	0.5	24	465	0.8/3.3	1.621	33
C_3S-DFFL[a]	0.5	24	484	0.4/1.9/3.5	1.344	49[a]
C_3S-DFFL[a]	0.5	24	506	0.25/1.4/3.3	1.336	54[a]

[a] To decrease the size of the parameter $\chi 2$, describing the quality of the resulting fit, we also performed a triexponential fit. The relative concentrations of the components with the two shortest lifetimes are marked with an asterix* for a better distinction (see equation (5)).

tables 6 and 7, do not arise from changes in ionic strength and in pH value.

Based upon tables 5–7 and literature data on the processes occurring during the hydration of the main cement phases (C_3A and C_3S) and of white cement, we subsequently derived possible explanations the behaviour of DFFL in the different pastes.

Q-DFFL pastes

The good match between the absorbance and fluorescence properties and the fluorescence decay kinetics of DFFL in the Q pastes and in dye solution suggests a similar environment of the dye molecules in both samples. Apparently, the DFFL molecules remain surrounded by water molecules between the Q-grains (see figure 7). An interaction of the dye molecules with surfaces of the Q-grains can be excluded in basic solution. This assumption is also supported by the negative zeta potential of quartz surfaces found by Ferrari *et al* [82]., which should favor electrostatic repulsion of the dye molecules.

C_3A-DFFL pastes

In the C_3A-DFFL pastes, the strongest changes in the absorbance of DFFL occur already in the freshly prepared pastes (t = 0 h) (see figure). 6 Normalized absorbance spectra (KM) of the pastes prepared from Q (first row, left), C_3A (first row, right), C_3S (second row, left), and WC (second row, right) at different times of hydration and the absorbance spectrum of DFFL in saturated $Ca(OH)_2$ solution (dashed line). The measurements were done with a cut-off filter of 525 nm.) and the fluorescence decay kinetics become biexponential. This could suggest the formation of non-emissive dye aggregates [83], caused by an enhanced local dye concentration, favored by hydration-induced water-consumption [19, 20, 26]. This assumption is supported by the fast reaction of pure tricalcium aluminate with water yielding metastable calcium aluminate hydrates C_4AH_{13} or with more water C_4AH_{19}, which converts to cubic hydrogarnet (C_3AH_6) [24, 84, 85], summarized as C–A–H phases in the following. C–A–H can be optically detected by a characteristic absorbance band at 1400 nm in the reflectance spectra originating from bound water molecules [86] as shown in the SI (see figure S6), The prompt consumption of water by C_3A becomes already obvious during the preparation of the C_3A paste, where twice the amount of solution was necessary for the formation of a homogeneous paste. However, as shown in figure S2 in the SI, DFFL dimerization requires a local dye concentration of at least $2.5 * 10^{-2}$ mol l^{-1}, exceeding the initial DFFL concentration ($3.2 * 10^{-4}$ mol l^{-1}) by a factor of hundred, requiring that 99% of the initially present water molecules have meanwhile reacted with C_3A or adsorbed at C_3A. Also, DFFL dimerization leads to an increase in the absorbance at 465 nm (see figure S2).

Table 5. Possible effects affecting the optical properties of a reporter dye.

Effect	Absorbance	Fluorescence
(a) Interaction of the dye with particle surfaces	Change in the band shape [29, 65, 66] and spectral position [29]	Change in spectral shape [29, 65] and spectral position of the fluorescence band [29, 65, 66]
(b) Dye-dye interactions and dye aggregation	Change in spectral shape of the absorbance band like a broadening of the main absorbance band, often an enhancement of the vibronic shoulder, possibly an apparent change in the spectral position of the main absorbance band [22, 65, 73, 75, 76]	Fluorescence quenching [73, 75, 76]
(c) Change in ionic strength of dye microenvironment	Change in spectral shape like a broadening of the main absorbance band, enhancement of vibronic shoulders and/or appearance of new bands [49] and change in spectral band position [78, 80, 81]	Increase [79] or reduction [80] of fluorescence intensity; spectral position and shape of the fluorescence band often remain unaffected; possible change in fluorescence decay kinetics
(d) pH-value (important for pH-responsive DFFL at pH-values < 6)	Change in spectral shape and spectral position of the absorbance maximum [47–49]	Additional shoulders in the long wavelength region [47–49], no change of the spectral position of the fluorescence maximum

Table 6. Main optical changes of DFFL in the different pastes in comparison to DFFL in solution at time t = 0 h as discussed in the previous sections (see, e.g. figure 6 and tables 2–4).

Paste	Absorbance spectra	Fluorescence spectra	Decay kinetics
Q-DFFL	Slight signal broadening and slight enhancement of the vibronic shoulder	Bathochromic shift of 4 nm	Similar behavior as observed for DFFL in solution
C_3A-DFFL	Strong change in signal shape and maximum (462 nm)	Bathochromic shift of 4 nm	Bi-exponential decay kinetics, shortening of lifetime
C_3S-DFFL	Signal broadening, bathochromic shift of the maximum of 4 nm	Bathochromic shift of 7 nm	Bi-exponential decay kinetics, shortening of lifetime
WC-DFFL	Signal broadening	Bathochromic shift of 5 nm	Similar behavior as observed for DFFL in solution

The loss in absorbance intensity (KM) of DFFL (see figure 5) with time, that occurs only in the C_3A-DFFL pastes, points to a partial decomposition of DFFL in this paste, possibly promoted by interaction with the C_3A– or C–A–H-surfaces. DFFL-C3A shows tri-exponential decay kinetics after a hydration time of 24 h. Hence, different effects seem to be the responsible for the observed spectroscopic changes as the appearance of a second emissive species with a significantly shorter lifetime below 3 ns suggests additionally an interaction of the DFFL molecules with the C–A–H surfaces (see figure 7).

C_3S-DFFL pastes

The bathochromic shifts of the absorbance (KM) and fluorescence bands of DFFL in C_3S-DFFL pastes at t = 0 h together with the broadened absorbance signal, lacking, however, the pronounced vibronic shoulder typical for dye aggregates (see also figure S2), indicate a rapid interaction of the negatively charged dye with the C_3S surfaces. The postulated interaction of DFFL with C3S surfaces is in a good agreement with observations of Shi *et al* [66] and Constantino *et al* [65], revealing a positive zeta potential of C_3S in pore or hydroxide solution [52, 54]. Such dye-surface interactions could account for the reduced fluorescence intensity (see figure 2), and the shortened fluorescence lifetimes (see table 4) as well as the triexponential fluorescence decay kinetics.

Hydration of C_3S [87–89] includes four hydration stages, namely the initial dissolution, the induction period, the acceleration period, and the deceleration period. The reaction rate of C_3S with water and the formation of calcium silicate hydrates (C–S–H) with a defective tobermorite-like structure [19, 90–92] is particularly high 10 h after the onset of hydration [92, 93]. At this time, the splitting of the DFFL absorbance band (see figure 6) occurs accompanied by a significant reduction and broadening of the fluorescence signal. This could possibly be ascribed to the incorporation of DFFL into the Ca–H–O intermediate layers of C–S–H as previously reported for fluorescein [65, 66], leading to a bathochromically shifted absorbance band at 506 nm of these DFFL molecules.

WC-DFFL pastes

The absorbance (KM) and fluorescence spectra of DFFL in WC-DFFL at t = 0 h, that are identical with those of DFFL in the Q pastes and in basic aqueous solution, and the mono-exponential fluorescence decay suggests a location of the dye in the water phase. The strongly reduced fluorescence intensity (see figure 3) after 10 h and the observed bi-exponential decay kinetics are ascribed to the interaction of DFFL with C–S–H surfaces. The broadening of the absorbance (KM) signal accompanied by the appearance of shoulders at the longer (510 nm) and slightly delayed also at the shorter flank (450 nm) of the absorption band are attributed to an increasing number of dye molecules interacting with C–S–H surfaces as observed for the C_3S pastes, accompanied by a beginning dye aggregation favoured by water consumption during cement hydration. These explanations are depicted in figure 8.

To assess our hypothesis shown in figure 8, we subsequently compared the absorbance (KM) spectrum of DFFL in the WC paste obtained at t = 20 h (see figure 6) with the sum of the absorbance spectra (KM) of DFFL in the WC paste (t = 0 h), C_3A paste (t = 0 h), and C_3S paste (t = 20 h). Thereby, we model the presence of free DFFL molecules, aggregated dyes, and surface-adsorbed dyes or dye molecules incorporated into layered structures formed during hydration. The respective spectra derived from the different pastes were weighted prior to the calculation of the sum spectrum. The good match of the measured and calculated sum spectra shown in figure 9 confirms our assumption.

Conclusion and outlook

In summary, the time-dependent changes of the spectral position, shape, and intensity of the reflectance and fluorescence signals of the negatively charged reporter dye 2′,7′-difluorofluorescein (DFFL) and its fluorescence lifetime and decay kinetics were utilized to derive a deeper understanding of the structural changes on a molecular level, that accompany hydration processes in pastes of white cement, cubic tricalcium aluminate, and tricalcium silicate, the

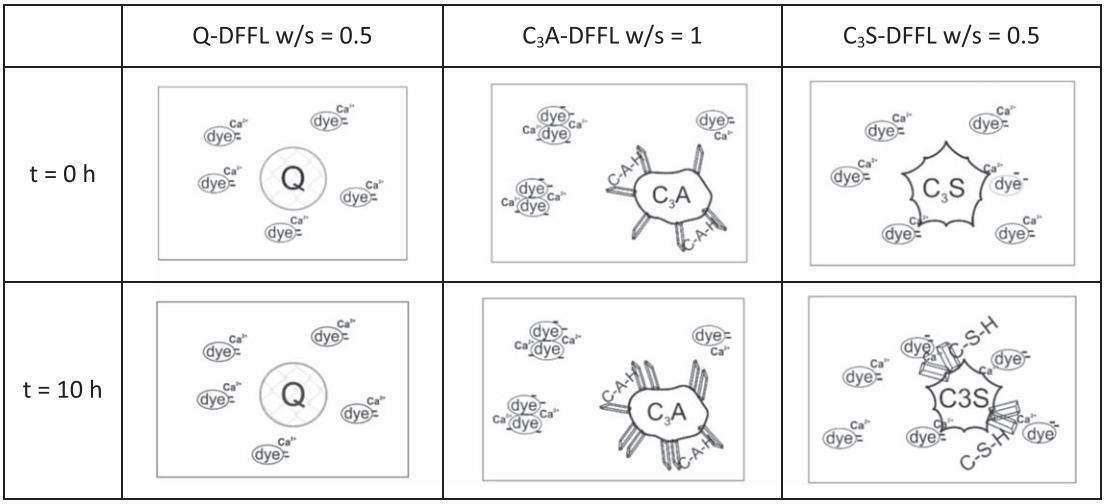

Figure 7. Schematic representation of the different types of interaction of DFFL in Q, C_3A, and C_3S pastes.

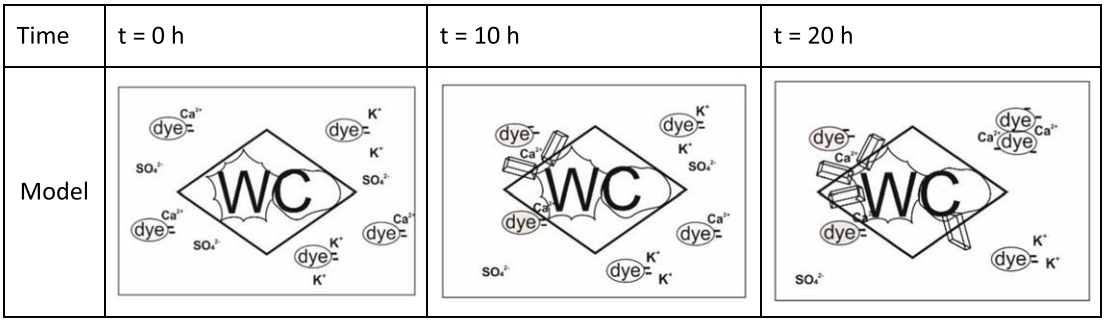

Figure 8. Schematic representation of the different types of interaction of DFFL in WC-DFFL pastes.

Table 7. Main optical changes of DFFL in pastes at time t = 24 h in comparison to DFFL in pastes in pastes at time t = 0 h as discussed in the previous sections (see, e.g. figures 3, 5, and 6 and tables 2–4).

Paste	Absorbance spectra	Fluorescence spectra	Decay kinetics
Q-DFFL	Similar behaviour as observed for Q-DFFL at t = 0 h	Reduced to 85% of the initial intensity	Similar behaviour as observed at t = 0 h; no dependence of the decay kinetics on excitation wavelength
C_3A-DFFL	Intensity reduced by 50%; slight decrease of the shoulder at 500 nm	Intensity reduced by 50%	Enhanced contribution of the components with short lifetimes; triexponential decay kinetics. Excitation at 500 nm yields a larger contribution of the components with short lifetimes
C_3S-DFFL	Splitting of the absorbance band into two peaks at 484 nm and 506 nm	Reduced to 20% of the initial intensity	Triexponential decay kinetics. Excitation at 506 nm yields larger contribution of the components with short lifetimes
WC-DFFL	Change in signal shape: two shoulders (450 nm/510 nm) in addition to the maximum at 484 nm	Reduced by 20% of the intensity	Tri-exponential decay kinetics; excitation at 510 nm yields the largest contribution of the components with the short lifetimes

main phases of cement, and in a paste of quartz filler. Based upon a comparison of these results and the results obtained by isothermal heat flow calorimetry and the consideration of literature data about time-dependent modifications of cement paste, we conclude that the dramatic reduction in DFFL fluorescence intensity in the WC-DFFL pastes is most likely caused by either the interaction of DFFL ions with C_3S– and C–S–H phases or by intercalation in C–S–H phases. Furthermore, with the aid of an optical reporter, also processes, that consume a large amount of initially present water can be identified utilizing spectroscopically detectable dye-dye interaction and dye aggregation favored by an increased local dye

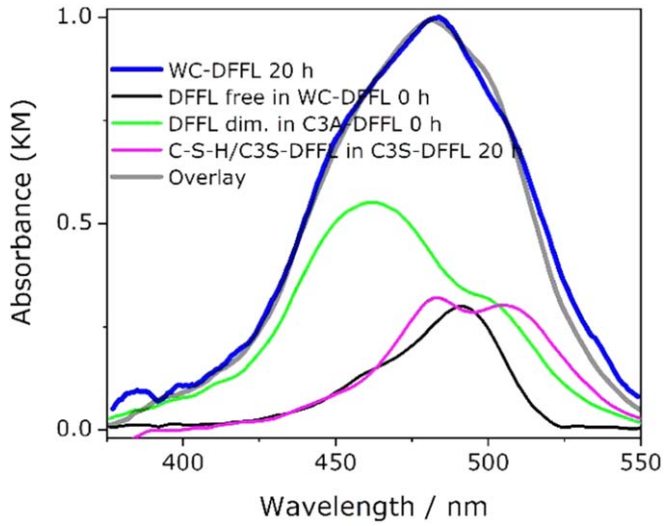

Figure 9. Comparison of the absorbance spectrum (KM) of DFFL measured in the WC-DFFL paste after 20 h (blue line) and a sum spectrum (gray line, overlay) calculated from the absorbance spectra (KM) of the free dye (Q-DFFL, t = 0 h; black line), aggregated dye (C_3A-DFFL, t = 0 h; green line), and the dye in the presence of C-S-H (C_3S-DFFL, t = 20 h; pink line).

concentration. In the future, we plan to extend these studies to a positively charged and a neutral fluorophore. In addition, we will perform optically monitored screening studies with different types of polycarboxylate ethers and other modern cement additives, utilizing also other conventional structure analytical methods.

Acknowledgments

The authors acknowledge financial support from the BAM-funded focus area project M-Flow. Furthermore, we acknowledge technical support by Sebastian Simon from division 7.4 of BAM for the *in situ* XRD analysis of the white cement used, and Matthias Michaelis from division 1.2 of BAM for the determination of the molar absorption coefficients.

The authors have declared that no conflicting interests exist.

Data availability statement

All data that support the findings of this study are included within the article (and any supplementary files).

ORCID iDs

U Resch-Genger https://orcid.org/0000-0002-0944-1115

References

[1] JCCS GLOBE - Global Consensus on Sustainability in the Built Environment [Online], Available at: https://rilem.net/article/globe-global-consensus-on-sustainability-in-the-built-environment-192 (Accessed: 20210331)
[2] Lehne J and Preston F 2018 *Chatham House Report*
[3] U. N. E. Programme 2020 Global Status Report for Buildings and Construction: Towards a Zero-emission, Efficient and Resilient Buildings and Construction Sector [Online], Available at: https://wedocs.unep.org/20.500.11822/34572 (Accessed: 20210331)
[4] Schmidt W 2014 Design Concepts for the Robustness Improvement of Self-Compacting Concrete *PhD Thesis* Eindhoven University of Technology
[5] Stroh J, Schlegel M C, Schmidt W, Nguyen Thi Y, Meng B and Emmerling F 2016 *Constr. Build. Mater.* **106** 18–26
[6] Locher F W, Richartz W and Sprung S 1976 *Zement-Kalk-Gips* **29** 435–42
[7] Locher F W, Richartz W and Sprung S 1980 *Zement-Kalk-Gips* **33** 271–7
[8] Schmidt W, Brouwers H J H, Kuhne H C and Meng B 2017 *Constr. Build. Mater.* **139** 584–93
[9] Hesse C, Goetz-Neunhoeffer F, Neubauer J, Degenkolb M and Gäberlein P 2008 *Cement International* **06** 68–78
[10] Hesse C, Goetz-Neunhoeffer F and Neubauer J 2011 *Cem. Concr. Res.* **41** 123–8
[11] Scrivener K L and Nonat A 2011 *Cem. Concr. Res.* **41** 651–65
[12] Hesse C, Goetz-Neunhoeffer F, Neubauer J, Braeu M and Gaeberlein P 2009 *Powder Diffr.* **24** 112–5
[13] Le Saout G, Kocaba V and Scrivener K 2011 *Cem. Concr. Res.* **41** 133–48
[14] Schlegel M C, Sarfraz A, Muller U, Panne U and Emmerling F 2012 *Angewandte Chemie-International Edition* **51** 4993–6
[15] Skibsted J and Jakobsen H J 1998 Characterization of the Calcium Silicate and Aluminate Phases in Anhydrous and Hydrated Portland Cements by 27Al and 29Si MAS Spectroscopy *Nuclear Magnetic Resonance Spectroscopy of Cement-Based Materials* (Heidelberg: Springer) 1978-3-642-80432-8
[16] Andersen M D, Jakobsen H J and Skibsted J 2004 *Cem. Concr. Res.* **34** 857–68
[17] Sun G K, Young J F and Kirkpatrick R J 2006 *Cem. Concr. Res.* **36** 18–29
[18] Alonso M D, Palacios M and Puertas F 2013 *Ind. Eng. Chem. Res.* **52** 17330–40
[19] Muller A C A, Scrivener K L, Gajewicz A M and McDonald P J 2013 *J. Phys. Chem.* C **117** 403–12

[20] Jansen D, Naber C, Ectors D, Lu Z, Kong X M, Goetz-Neunhoeffer F and Neubauer J 2018 *Cem. Concr. Res.* **109** 230–42
[21] Higl J, Hinder D, Rathgeber C, Ramming B and Linden M 2021 *Cem. Concr. Res.* **142** 106367
[22] Tarrida M, Madon M, Lerolland B and Colombet P 1995 *Adv. Cem. Based Mater.* **2** 15–20
[23] Kirkpatrick R J, Yarger J L, McMillan P F, Yu P and Cong X D 1997 *Adv. Cem. Based Mater.* **5** 93–9
[24] Black L, Breen C, Yarwood J, Phipps J and Maitland G 2006 *Advances in Applied Ceramics* **105** 209–16
[25] Jansen D, Goetz-Neunhoeffer F, Stabler C and Neubauer J 2011 *Cem. Concr. Res.* **41** 602–8
[26] Scrivener K L, Juilland P and Monteiro P J M 2015 *Cem. Concr. Res.* **78** 38–56
[27] Ramirez A, Pauli J, Crasselt C, Simon S, Schmidt W and Resch-Genger U 2021 *Constr. Build. Mater.* **270** 121857
[28] Ramirez A, Pauli J, Mota B, Casselt C, Simon S, Schmidt W and Resch-Genger U 2020 *Cem. Concr. Res.* **133** 106082
[29] Grabolle M, Starke M and Resch-Genger U 2016 *Langmuir* **32** 3506–13
[30] Resch-Genger U, Grabolle M, Cavaliere-Jaricot S, Nitschke R and Nann T 2008 *Nat. Methods* **5** 763–75
[31] Bigall N C, Parak W J and Dorfs D 2012 *Nano Today* **7** 282–96
[32] van der Vlist E J, Nolte-'t Hoen E N M, Stoorvogel W, Arkesteijn G J A and Wauben M H M 2012 *Nat. Protoc.* **7** 1311–26
[33] Licha K and Resch-Genger U 2011 *Drug Discovery Today* **8** 87–94
[34] Maurice D M 1967 *Invest Ophthalmol* **6** 464–77 https://iovs.arvojournals.org/
[35] Kwan A S L, Barry C, McAllister I L and Constable I 2006 *Clinical and Experimental Ophthalmology* **34** 33–8
[36] Bujdak J 2006 *Appl. Clay Sci.* **34** 58–73
[37] Connors K A and Jozwiakowski M J 1987 *J. Pharm. Sci.* **76** 892–7
[38] Jozwiakowski M J and Connors K A 1988 *J. Pharm. Sci.* **77** 241–6
[39] Polette-Niewold L A, Manciu F S, Torres B, Alvarado M and Chianelli R R 2007 *J. Inorg. Biochem.* **101** 1958–73
[40] Hashemian S 2007 *Main Group Chemistry* **6** 97–107
[41] Catanese C A 2017 *Color Atlas of Forensic Medicine and Pathology* (Boca Raton, FL: CRC Press) 978-1-4665-8591-1
[42] Leung B O and Chou K C 2011 *Appl. Spectrosc.* **65** 967–80
[43] Giloh H and Sedat J W 1982 *Science* **217** 1252–5
[44] Sato K *et al* 2016 *Bioconjugate Chem.* **27** 404–13
[45] Bujdak J and Komadel P 1997 *J. Phys. Chem.* B **101** 9065–8
[46] Sun W C, Gee K R, Klaubert D H and Haugland R P 1997 *J. Org. Chem.* **62** 6469–75
[47] Orte A, Crovetto L, Talavera E M, Boens N and Alvarez-Pez J M 2005 *J. Phys. Chem.* A **109** 734–47
[48] Martin M M and Lindqvist L 1975 *J. Lumin.* **10** 381–90
[49] Sjoeback R, Nygren J and Kubista M 1995 *Spectrochimica Acta Part a-Molecular and Biomolecular Spectroscopy* **51** L7–21
[50] Magde D, Wong R and Seybold P G 2002 *Photochem. Photobiol.* **75** 327–34
[51] Plank J and Hirsch C 2007 *Cem. Concr. Res.* **37** 537–42
[52] Zingg A, Winnefeld F, Holzer L, Pakusch J, Becker S and Gauckler L 2008 *J. Colloid Interface Sci.* **323** 301–12
[53] Mollah M Y A, Adams W J, Schennach R and Cocke D L 2000 *Advances in Cement Research* **12** 153–61
[54] Kong X M, Emmerling S, Pakusch J, Rueckel M and Nieberle J 2015 *Cem. Concr. Res.* **75** 23–41
[55] Suzuki K, Nichikawa T, Kato K, Hayashi H and Ito S 1981 *Cem. Concr. Res.* **11** 759–64
[56] Putz D H (2019) Match! Phase Identification from Powder Diffraction *Crystal Impact*
[57] Kubelka P 1948 *J. Opt. Soc. Am.* **38** 448–57
[58] Kubelka P 1948 *J. Opt. Soc. Am.* **38** 1067–1067
[59] Kortüm G, Braun W and Herzog G 1963 *Angewandte Chemie, International Edition* **2** 333–41
[60] Kortüm G 1966 *Reflectance Spectroscopy Principles, Methods, Applications* (Berlin, Heidelberg: Springer) (https://doi.org/10.1007/978-3-642-88071-1_5)
[61] Simmons E L 1975 *Appl. Opt.* **14** 1380–6
[62] Frei R W 1976 *Journal of Research of the National Bureau of Standards Section a-Physics and Chemistry* **80** 551–65
[63] Ramírez A, Pauli J, Mota B, Crasselt C, Simon S, Schmidt W and Resch-Genger U 2020 *Cement and Concrete Research* **133** 106082
[64] Rurack K, Hoffmann K, Al-Soufi W and Resch-Genger U 2002 *J. Phys. Chem.* B **106** 9744–52
[65] Costantino U, Coletti N, Nocchetti M, Aloisi G G, Elisei F and Latterini L 2000 *Langmuir* **16** 10351–8
[66] Shi W, Sun Z, Wei M, Evans D G and Duan X 2010 *J. Phys. Chem.* C **114** 21070–6
[67] Lakowicz J R 2006 *Principles of Fluorescence Spectroscopy* 3rd edn (Boston: Springer) (https://doi.org/10.1007%2F978-0-387-46312-4)
[68] Lopez S G, Crovetto L, Alvarez-Pez J M, Talavera E M and Roman E S 2014 *Photochemical & Photobiological Sciences* **13** 1311–20
[69] del Monte F and Levy D 1998 *J. Phys. Chem.* B **102** 8036–41
[70] Jelley E E 1936 *Nature* **138** 1009–10
[71] Scheibe G 1938 *Kolloid-Zeitschrift* **82** 1–14
[72] Eisfeld A and Briggs J S 2006 *Chem. Phys.* **324** 376–84
[73] Foerster T and Koenig E 1957 *Zeitschrift für Elektrochemie, Berichte der Bunsengesellschaft für physikalische Chemie* **61** 344–8
[74] Lavorel J 1957 *J. Phys. Chem.* **61** 1600–5
[75] Arbeloa I L 1981 *Journal of the Chemical Society-Faraday Transactions 2: Molecular and Chemical Physics* **77** 1725–33
[76] Arbeloa I L 1983 *Dyes Pigm.* **4** 213–20
[77] Grabolle M, Pauli J, Brehm R and Resch-Genger U 2014 *Dyes Pigm.* **103** 118–26
[78] Lubbers D W and Opitz N 1983 *Sens. Actuators* **4** 641–54
[79] Cortese J D, Voglino A L and Hackenbrock C R 1991 *J. Cell Biol.* **113** 1331–40
[80] Xiang J F, Yang X R, Chen C P, Tang Y L, Yan W P and Xu G Z 2003 *J. Colloid Interface Sci.* **258** 198–205
[81] Slavnova T D, Chibisov A K and Gorner H 2005 *J. Phys. Chem.* A **109** 4758–65
[82] Ferrari L, Kaufmann J, Winnefeld F and Plank J 2010 *J. Colloid Interface Sci.* **347** 15–24
[83] Arbeloa I L 1981 *Journal of the Chemical Society-Faraday Transactions 2: Molecular and Chemical Physics* **77** 1735–42
[84] Minard H, Garrault S, Regnaud L and Nonat A 2007 *Cem. Concr. Res.* **37** 1418–26
[85] Quennoz A and Scrivener K L 2012 *Cem. Concr. Res.* **42** 1032–41
[86] Watanabe A, Furukawa H, Miyamoto S and Minagawa H 2019 *Constr. Build. Mater.* **196** 95–104
[87] Bullard J W, Jennings H M, Livingston R A, Nonat A, Scherer G W, Schweitzer J S, Scrivener K L and Thomas J J 2011 *Cem. Concr. Res.* **41** 1208–23
[88] Pustovgar E, Sangodkar R P, Andreev A S, Palacios M, Chmelka B F, Flatt R J and De Lacaillerie J-B D E 2016 *Nat. Commun.* **7** 10952
[89] Scrivener K, Ouzia A, Juilland P and Mohamed A K 2019 *Cem. Concr. Res.* **124** 105823
[90] Richardson I G 2004 *Cem. Concr. Res.* **34** 1733–77
[91] Allen A J, Thomas J J and Jennings H M 2007 *Nat. Mater.* **6** 311–6
[92] Lothenbach B and Nonat A 2015 *Cem. Concr. Res.* **78** 57–70
[93] Richardson I G 2008 *Cem. Concr. Res.* **38** 137–58